$Cu(In,Ga)Se_2$ solar cells on low cost mild steel substrates

Lucas Zortea[1], Shiro Nishiwaki[1], Thomas Paul Weiss[1], Stefan Haass[1], Julian Perrenoud[2], Lukas Greuter[1], Thomas Feurer[1], Ganesan Palaniswamy[3], Stephan Buecheler[1*] and Ayodhya N. Tiwari[1]

[1]Laboratory for Thin Films and Photovoltaics, Empa – Swiss Federal Laboratories for Materials Science and Technology, Ueberlandstrasse 129, 8600 Duebendorf, Switzerland

[2]Flisom AG - Switzerland

[3]Tata Steel - Netherlands

*E-Mail: Stephan.buecheler@empa.ch

This document is the accepted manuscript version of the following article: Zortea, L., Nishiwaki, S., Weiss, T. P., Haass, S., Perrenoud, J., Greuter, L., ... Tiwari, A. N. (2018). $Cu(In,Ga)Se_2$ solar cells on low cost mild steel substrates. *Solar Energy*. http://doi.org/10.1016/j.solener.2017.12.057

Abstract

Thin film Cu(In,Ga)Se_2 (CIGS) solar modules can be grown on flexible and lightweight substrates allowing their direct integration into building elements. Such multifunctional building elements would significantly reduce the installation cost of photovoltaic systems provided that CIGS solar cells with high conversion efficiency can be obtained. Also, there is a need for low cost substrate foil. Mild steel is a promising low cost substrate material due to its excellent mechanical stability and already wide acceptance as component in building envelopes and in numerous other applications. During the growth of the CIGS absorber layer certain elements, e.g. iron, can diffuse from the metallic substrate into the semiconductor deteriorating the device performance. Here we present an effective diffusion barrier and device architecture for processing of highly efficient CIGS solar cells on mild steel substrates. The CIGS absorber layers were grown on mild steel foils by a multistage co-evaporation process at different substrate temperatures. The mild steel substrates were plated with an industrially scalable electrodeposited Ni/Cr bi-layer. The diffusion barrier layer properties of this Ni/Cr coating were investigated directly by measuring the metallic impurities within the absorber by secondary ion mass spectrometry and indirectly by admittance spectroscopy. The Ni/Cr bi-layer was found to be effective up to a nominal CIGS growth temperature of 500 °C. A certified cell efficiency of 18.0 % was achieved on a Ni/Cr coated mild steel substrate using a low temperature CIGS deposition process and a NaF and RbF post deposition treatment method.

Keywords

CIGS thin films, flexible solar cells, steel, diffusion barrier, roll-to-roll

1 Introduction

The efficiency of $Cu(In,Ga)Se_2$ (CIGS) thin film solar cells has increased in the past years and a maximum conversion efficiency of 22.6 % for CIGS on a rigid glass substrate was achieved (Jackson et al., 2016) by using improved alkaline post deposition treatments. With process modifications CIGS solar cells can also be fabricated on flexible and lightweight substrates e.g. stainless steel, aluminum or polyimide foil which facilitates cost effective roll-to-roll production. Lightweight and flexible solar modules offer several advantages for building integrated photovoltaics compared to rigid and rather heavy glass-glass laminated counterparts. Such modules can for example be integrated on rooftops where heavy photovoltaic systems cannot be installed due to weight restrictions and not flexible form factor for curved surfaces. In addition, the high fraction of installation costs of photovoltaic systems might be bypassed by direct integration of solar cells into building elements. Flexible and lightweight solar modules are also attractive for integration on transport vehicles, such as cars, trucks, trains and airships.

Mild steel is one of the most promising substrate materials for building integrated photovoltaics due to its high prevalence in construction e.g. as base material for façade elements or roof tiles as well as in transport vehicles. The excellent mechanical stability and the intrinsic barrier properties against water vapor are additional benefits for the applications in buildings. The main benefit of a mild steel substrate would be its low cost compared to stainless steel substrates and its superior mechanical and temperature stability compared to polyimide substrates. The highest reported efficiency of 20.4 % for flexible CIGS has been achieved on polyimide substrates (Chirila et al., 2013) but our group has also reported efficiencies of 17.7 % on stainless steel and 17.1 % on aluminum foils (A. Chirila, 2011). On mild steel substrates efficiencies of 12.8 % (Wuerz et al., 2009) and 14.5 % (A. Chirila, 2011) were reported for co-evaporated CIGS solar cells.

The performance of CIGS solar cells on mild steel has not been taped to its full potential yet as some of the problems need further investigation and development work. In

particular the diffusion of detrimental elements from the steel substrate into the semiconductor during solar cell processing at high temperatures is so far an unsolved problem. The photovoltaic (PV) performance of CIGS solar cells on steel substrates can be adversely affected by the diffusion of impurities from the substrate material or protection coatings into the absorber material. Stainless steel is commonly alloyed with nickel and chromium in order to increase the corrosion resistance. Also mild steel needs additional corrosion protection which can be achieved by plating dense nickel or chromium layers. Eisenbarth (Eisenbarth et al., 2012) et al. and Wuerz et al. (Wuerz et al., 2014) previously described the detrimental influence of iron on the device perfomance. Furthermore, the impact of nickel and chromium impurites was recently investigated (Pianezzi et al., 2015). These impurities are described to form electrically active defect states within the energy bandgap of the absorber causing additional recombination losses in the device. Metallic e.g. Ti/TiN (Liu et al., 2015) (Blosch et al., 2011), Cr (Cho et al., 2013) and oxide based e.g. Al_20_3 (Bae et al., 2013; Herz et al., 2003) barrier layers can prevent elemental migration from the steel substrate and hence mitigate electrical performance losses. Using low substrate temperatures during CIGS co-evaporation on stainless steel was also shown to be an effective alternative to barrier layers for reducing the impurity diffusion (Pianezzi et al., 2012). We have investigated an industrially scalable Ni and Cr based corrosion protection and elemental diffusion barrier layer on mild steel foil for the development of CIGS solar cells. Here, we demonstrate that highly efficient flexible solar cells can be obtained on mild steel with slight modifications of the CIGS deposition process. Using secondary ion mass spectrometry (SIMS) and admittance spectroscopy we show that the diffusion of detrimental elements from the substrate is sufficiently suppressed by the Ni/Cr double layer. Since Ni and Cr impurities themselves are known to deteriorate the cell performance a TiN diffusion barrier was applied in selected cases in order to investigate if additional impurity protection is necessary at high substrate temperatures. A certified efficiency of 18.0 % was achieved on Ni/Cr plated mild steel us-

ing a low temperature deposition process and a RbF post deposition treatment without an additional TiN diffusion barrier layer.

2 Experimental

2.1 Device fabrication

Roll to roll produced mild steel substrates with a mirror surface finish (low-carbon steel with C<0.08 %, roughness R_a < 0.10 µm, thickness d=400 µm) were cleaned with an alkali solution, rinsed with deionized water, pickled with sulphuric acid (98 % purity, reagent grade) and again rinsed with deionized water. After the cleaning procedure the substrates were immediately taken into the electroplating bath. About 2 µm of nickel was plated at 55 °C with a current density of ~5 A/dm^2 using established Watts nickel bath (Nickel(II)sulphate (270 g/l), Nickel(II)Chloride (50 g/l), Boric Acid (30 g/l), wetting agent). Subsequently about 0.1 µm Chromium was plated through trivalent route using commercial baths (Trilyte® electrolyte provided by Enthone or TriChrome® Plus electrolyte provided by Atotech. The iron component (corrector) from this bath was replaced with KCl (20 g/l))

The substrates were rinsed with isopropanol and cleaned for 10 min using oxygen plasma (10 min) prior to coating with a 600 nm thick triple-layer molybdenum back contact by direct current (DC) magnetron sputtering.

CIGS absorber layers were deposited by a multistage co-evaporation method at different nominal substrate temperatures LT (400 °C), STD (450 °C), HT (500 °C), MAX (550 °C). With STD (450°C) corresponding to the standard low temperature process for polyimide substrates in our lab. The substrate temperature values were measured with a thermocouple placed behind the substrate. For all samples NaF postdeposition treatments (PDT) were applied and for the champion cell a NaF and RbF PDT was carried out. The details of the CIGS deposition and the postdeposition treatments are given elsewhere (Nishiwaki et al., 2017),(Chirila et al., 2013). Devices were finished by

a chemical bath deposited CdS buffer layer of about 50 nm thickness and a double layer of radio frequency (RF) magnetron sputtered ZnO (50 nm) and an aluminum doped ZnO (200 nm) as a front contact. Finally, a nickel/aluminum (50 nm/4000 nm) e-beam evaporated metallic grid was deposited trough a mask. The cell area was defined by mechanical scribing.

In selected cases an additional TiN diffusion barrier layer was applied between the substrate and the molybdenum back contact. The TiN diffusion barrier layer was composed of a DC magnetron sputtered (Ar=21 sccm, $p=8.5*10^{-3}$, Power density=2 W/cm^2) 20 nm thick Ti adhesion layer and a DC magnetron sputtered (Ar=21 sccm, N_2=10 sccm, $p=5*10^{-3}$mbar, Power density=3W/cm^2) 250 nm TiN layer. Devices processed with additional TiN impurity barrier layers are labeled as HT TiN and MAX TiN.

2.2 Characterization

The solar cells were characterized using current density-voltage (J-V) measurements under simulated standard test conditions (25 °C, 1000 W/m^2, AM1.5G). J-V curves were acquired using four point probe measurements on a Keithley 2400 sourcemeter. Independently certified measurements were performed by the Fraunhofer Institute ISE, Freiburg, Germany.

Elemental depth profiles of the full devices were obtained with a time-of-flight secondary ion mass spectrometry (ToF-SIMS) system from ION-TOF. Bi^+ ions were used as primary ions and positive secondary ions were detected. Sputtering was performed using O_2^+ sputtering ions with 2 keV ion energy, 400 nA ion current and a 300 × 300 μm^2 raster size. An area of 100 × 100 μm^2 was analyzed using Bi^+ ions with 25 keV ion energy.

The roughness of the coated substrates (S_a=85 nm) was determined with a 3D microscope (Leica, DCM8) using white light interferometry. The surface roughness was determined on a 600 x 800 μm^2 large area.

The active area quantum efficiency (EQE) was measured using a chopped light signal of a halogen lamp separated in a double grating monochromator. A halogen lamp bias with about 0.2 sun intensity was applied during the measurements. Admittance spectroscopy was used to identify energetic defects levels in the device. The capacitance was measured with a four point probe measurement using an Agilent E4980A LCR meter (Agilent Technologies Inc., Santa Clara, CA, USA) in the frequency range from 200 Hz to 2 MHz with 30 mV modulation amplitude. The temperature of the device was varied from 123 K to 323 K in a cryostat cooled with liquid nitrogen. All samples were stored in dark prior to the AS measurement for at least 1 h at 323 K to assure a relaxed state. A halogen lamp (100 W) served as illumination source for temperature dependent J-V measurements. The intensity of the halogen lamp was increased until the current density was equivalent to the one measured under standard test conditions.

3. Results

3.1 CIGS growth at different substrate temperatures on mild steel substrates

Figure 1 compares the PV parameters of CIGS solar cells grown at different nominal substrate temperatures LT, STD, HT and MAX. Also shown are the corresponding cells with additional TiN diffusion barrier HT TiN and MAX TiN. The V_{OC} of solar cells LT and LT TiN is low (~615 mV). For cells STD, HT, HT TiN and MAX TiN the V_{OC} increased to ~650 mV. Similar trends are observed for the fill factor and the conversion efficiency. The J_{SC} values of LT and STD are only slightly affected by the different processing temperatures and can be considered similar. Samples HT, HT TiN and MAX TiN show higher J_{SC} values compared to cells LT and STD.
For sample MAX a severe drop of all PV parameters is observed: (ΔV_{OC} ~ 60 mV), (ΔFF ~ 5 %), (ΔJ_{SC} = 3 mA/cm^2) resulting in about 4 abs % lower efficiency. This drop is not observed if an additional TiN diffusion barrier layer is applied.

Figure 2 compares the EQE of CIGS solar cells processed at different nominal substrate temperatures. Sample STD and HT (Fig 2a) and Sample HT and HT TIN (Fig 2c) show a similar spectral response. Samples HT, HT TiN and MAX TiN show additional carrier collection in the near infrared region compared to samples LT and STD (Fig 2b). The sample MAX shows a strongly decreased spectral response for $\lambda > 550$ nm compared to sample MAX TiN (Fig 2d). The extra carrier collection for samples HT, HT TiN and MAX TiN can be explained with additional photon absorption in the near infrared region due to a lower optical bandgap. Table 1 shows the minimum optical bandgaps for cells processed at different nominal substrate temperatures determined from the measured EQE (inflection point). Also shown are the calculated short circuit current densities determined from the spectral response ($J_{SC\ EQE}$). For sample MAX a severe drop in the $J_{SC\ EQE}$ is observed.

Tab. 1 Minimum optical bandgap determination for CIGS absorber layers grown at different nominal substrate temperatures. LT (nominal 400 °C), STD (nominal 450 °C), HT and HT TiN (nominal 500 °C) and MAX and MAX TiN (nominal 550 °C).

Sample	LT	STD	HT	HT TIN	MAX	MAX TIN
Bandgap (eV)	1.16	1.19	1.13	1.13	1.14	1.13
$J_{SC\ EQE}$ (mA/cm^2)	32.3	31.8	34.1	34	29.5	33

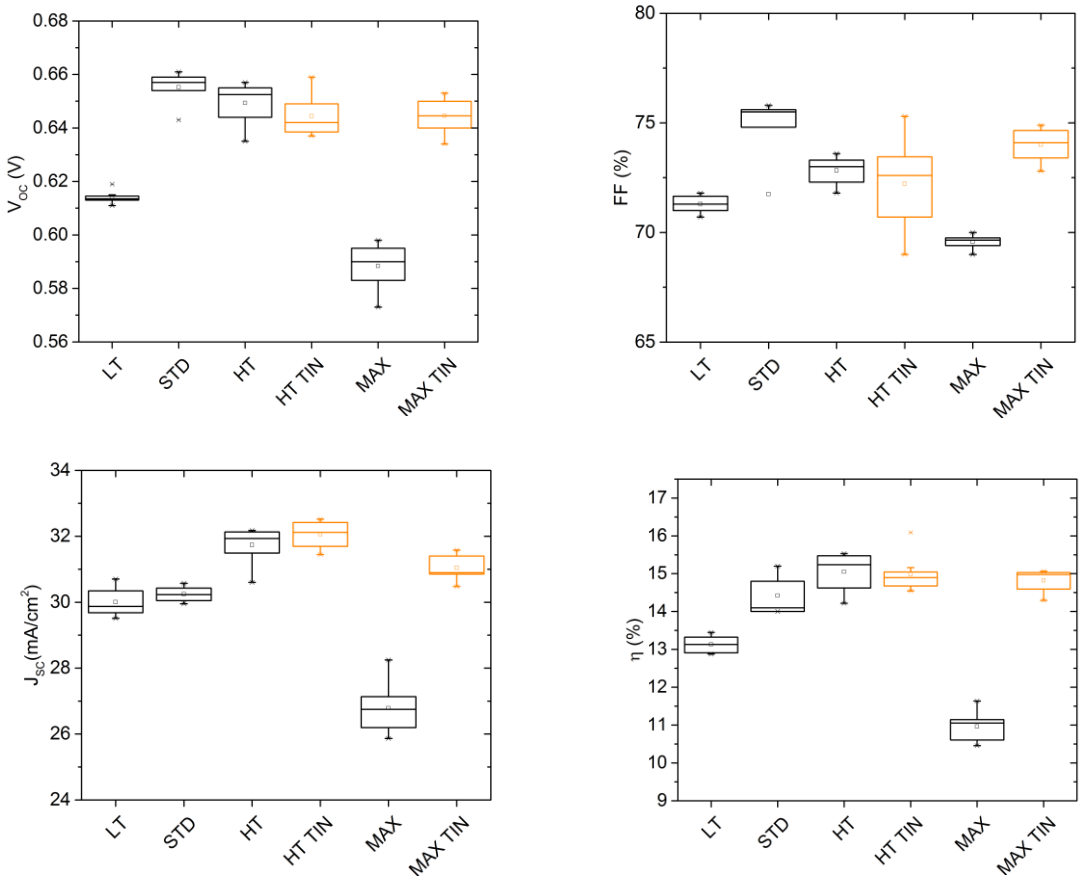

Fig 1. PV parameters of solar cells on barrier coated mild steel substrates with CIGS absorbers grown at different substrate temperatures LT and LT TiN (nominal 400 °C), STD and STD TiN (nominal 450 °C), HT and HT TiN (nominal 500 °C) and MAX (nominal 550 °C). The samples only have a NaF post deposition treatment and no MgF anti-reflection coating was used. On sample HT TiN the distribution of the FF is very broad compared to all other samples. The fluctuation

is caused by a large variation of the parallel resistance in the devices. The devices in this study were developed with only NaF-PDT and no MgF anti-reflection coating.

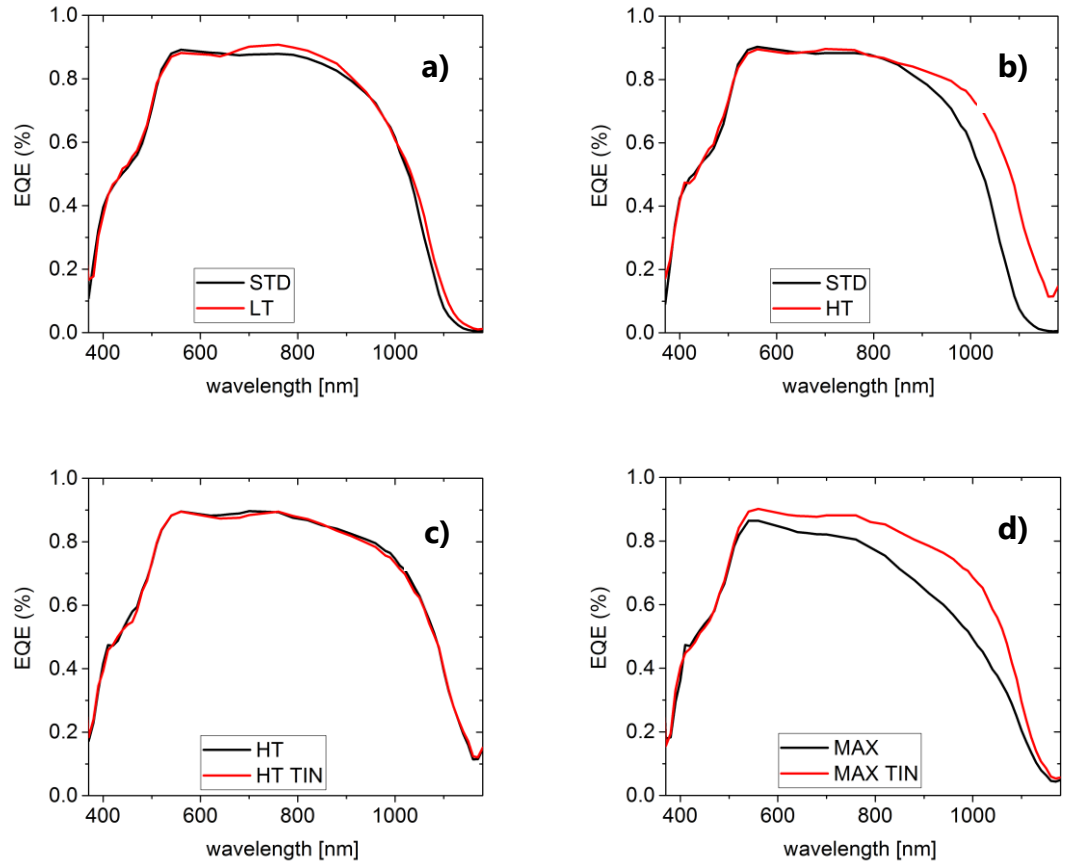

Fig. 2 Spectral response (EQE) of CIGS solar cells grown at different nominal substrate temperatures LT (nominal 400 °C), STD (nominal 450 °C), HT (nominal 500°C) and MAX (nominal 550 °C). Samples STD and LT (a) and samples HT and HT TiN show a similar spectral response. Additional carrier collection in the near infrared region for sample HT compared to STD is shown in (b). Carrier collection losses for sample MAX compared to MAX TiN is shown in (d).

Charge carrier collection losses toward longer wavelengths for CIGS grown on steel substrates were also observed in earlier studies (Wuerz et al., 2014). These carrier collection losses were described to increase with higher Fe impurity content within the

absorber. However, also Ni and Cr impurities within the CIGS absorber are known to strongly affect the spectral response for λ > 550 nm (Pianezzi et al., 2015). Furthermore, these impurities are known to form active defect states within the energy bandgap of the absorber and hence lead to non-radiative recombination losses and hence a decrease in V_{OC} and overall cell performance.

Based on these results it can be hypothesized that the barrier properties of the Ni/Cr bi-layer are sufficient if the nominal substrate temperature during CIGS processing does not exceed 500 °C. Furthermore, for higher substrate temperatures impurities diffused from the substrate (mild steel/Ni/Cr) through the Mo layer into the CIGS during processing cause additional non-radiative recombination losses which can be reduced by application of an additional TiN diffusion barrier layer. In the next sections these hypotheses are discussed.

3.2 Impurity diffusion at high temperatures

For the devices STD, MAX and MAX TiN elemental depth profiles using SIMS were measured in order to determine the impurity content within the CIGS absorber.
The presence of nickel, iron and chromium impurities was determined by integration of the measured elemental counts over the inner 50 % of the absorber layer.
In table 2 the absolute values of the integrated counts for each investigated impurity element and the copper reference are shown. The presence of nickel, chromium and iron within the inner 50 % of the absorber could not be clearly determined by SIMS due to the low number of measured counts. The measured elemental counts for these impurities are assigned to the noise of the method and are at the lower detection limit (LDL) of the measurement method and device morphology. An exception here is sample MAX where chromium can be detected within the absorber.

Tab. 2 Comparison of elemental counts using SIMS within the inner 50 % of the CIGS absorber for samples STD (nominal 450 °C) and MAX, and MAX TiN (nom-

inal 550 °C) measured with SIMS. The SIMS measurement for sample STD was acquired in a different measurement session but with the same nominal analyzing condition except for an increased raster size for the O_2^+ sputtering (400 × 400 µm^2). The star indicates signals which are over the determined detection limit.

	$STD_{inner50}$	$MAX_{inner50}$	$MAX\ TIN_{inner50}$
^{52}Cr	8	111 *	6
^{56}Fe	16	23	3
^{58}Ni	11	7	4
^{63}Cu	$9E^5$ *	$8E^5$ *	$8E^5$ *

3.3 Presence of active defect states

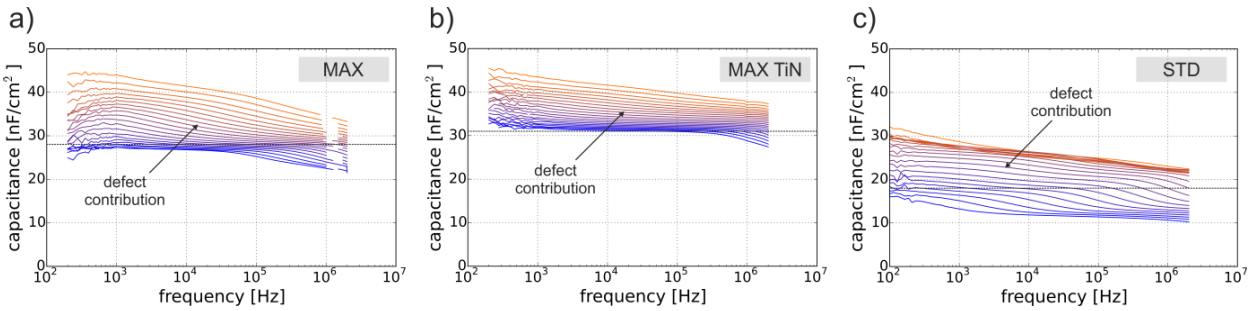

Fig. 3 Temperature dependent capacitance-frequency (C-f) measurements of devices with CIGS absorber grown at nominal 550°C (a and b) and 400°C (c). For MAX (a) a clear transition appears at high temperatures, which is almost absent for MAX TiN (b) (indicated by arrows). For the STD the transition appears at lowered temperatures (c). For sample MAX (a) some data points measured around 10^6 Hz which could be assigned to noise were removed for better visibility.

Admittance spectra were acquired on the samples: STD, MAX and MAX TiN in order to identify the presence of active defect states within the energy band gap of the absorber. These defect states might be caused by Ni, Cr (Pianezzi et al., 2015) or Fe impurities (Wuerz et al., 2014) (Pianezzi et al., 2012) and can lead to additional non-radiative recombination losses.

Figure 3 shows the capacitance-frequency curves determined from the admittance measurements in the temperature range of 123 to 323 K. The sample MAX shows a clear capacitance step at high temperatures with respect to frequency. MAX TiN indicates a similar transition in the same temperature range but with a smaller intensity i.e. a smaller capacitance drop. Such a capacitance step (indicated by the arrows in Fig 3a and b) might be caused by a deep defect state (Losee, 1975). At low frequencies the charging/discharging of the defect state can follow the alternate current (AC) modulation voltage and hence contributes to the capacitance. The capacitance contribution is lost at high frequencies where the modulation frequency is too fast for the defect state to be charged.

In contrast to the devices MAX and MAX TiN, the STD device (Fig 3c) shows two capacitance steps as well as an overall lower capacitance. The capacitance step at higher temperatures (indicated by the arrow in Fig 3c) might as well be due to a deep defect contribution. However, compared to the devices grown at 550 °C (MAX and MAX TiN) this capacitance step occurs at slightly lower temperatures (see also Fig. 4). The overall lower capacitance can be explained by a lower doping and built-in voltage as shown by the Mott-Schottky plot in Supplementary Figure A.

Additionally, a second capacitance step is observed at the lowest measured temperatures. In recent studies it was shown that this capacitance step might be due to a transport barrier in the device (Eisenbarth et al., 2010; Weiss et al., 2017; Werner et al., 2017).

3.4 Metal impurity contribution to deep defects

The evaluation as outlined by (Walter et al., 1996) has been applied in order to quantify the defect density N_t from the high temperature capacitance steps described in chapter 3.3 . In order to obtain a density of the defects over the complete energy range the defect signal has been fitted by a Gaussian distribution. The integrated area of the fit then gives the total defect density. The three defect spectra for sample STD, MAX and MAX TiN which were calculated from the capacitance step above the SCR capacitance are shown in Fig 4.

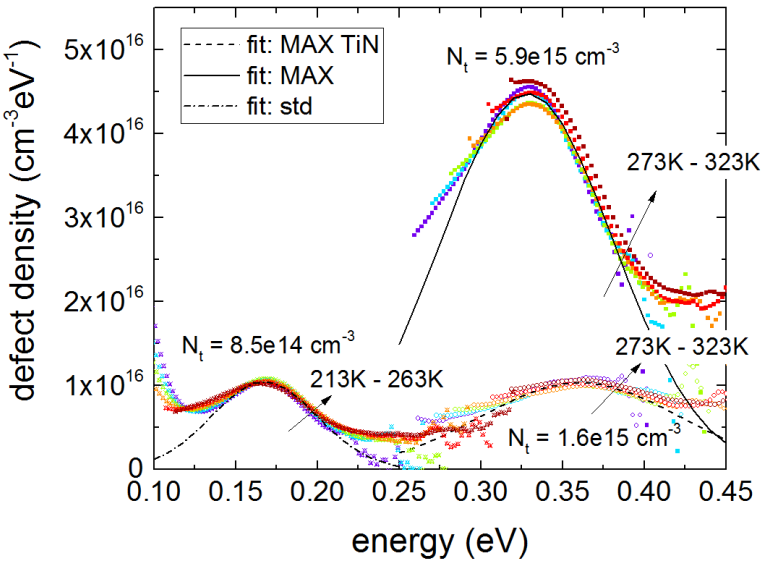

Fig. 4 Calculated defect spectra of MAX, MAX TIN and STD samples from the capacitance step (indicated by arrows) shown in Fig. 3.

Sample MAX exhibits a strong defect signal around 0.33 eV which could be assigned to impurities such as Ni, Cr or Fe (Pianezzi et al., 2012; Pianezzi et al., 2015; Wuerz et al., 2014). On sample MAX TiN the defect signal at a similar energy reduces considerably indicating a strong reduction of these defect states. The defect concentration is reduced roughly by a factor of 3.7 with the additional TiN barrier which explains the different device performances of MAX and MAX TiN described in chapter 3.1.

For nickel impurities in CIGS devices a distinct drop in capacitance down to the geometrical capacitance was observed earlier (Pianezzi et al., 2015) and a defect energy around 0.30 eV was assigned to this capacitance step. However, the capacitance step

for samples MAX and MAX TiN drops only to the space charge region capacitance. Furthermore, nickel could not be detected within the absorber using SIMS measurements. Consequently, we conclude that nickel impurities do not substantially contribute to the measured deep defect at 0.33 eV.

For chromium and iron impurities the energetic position of the corresponding deep defect level was previously determined around 0.30 eV (Pianezzi et al., 2012; Pianezzi et al., 2015). In this study a similar capacitance step shape in the same temperature and frequency range was observed and the defect around 0.33 eV is assigned to this specific transition. The SIMS measurements of these samples indicate that this defect is most likely caused by chromium impurities. However, due to the low presence of impurities within the device the contribution of chromium or even iron impurities to this deep defect remains ambiguous.

The sample STD does not exhibit the defect signal at 0.33 eV. It is concluded that STD does not contain the defect levels around 0.33 eV which might explain the high V_{oc} values for this device. In contrary, a low energy defect state around 0.17 eV with a defect concentration below 1e15 cm^{-3} was determined. However, the defect concentration and energy is rather low and cannot be assigned to any impurities.

Since no impurity related deep defect levels were found on sample STD we can conclude that the Ni/Cr bi-layer does sufficiently suppress the detrimental elemental migration from the substrate (mildsteel/Ni/Cr) into the CIGS absorber if the processing temperature does not exceed 500 °C. For higher substrate temperatures an additional TiN diffusion barrier is required in order to block the chromium and/or iron diffusion from the steel/Ni/Cr substrate.

3.5 Improvement of cell performance

Based on above findings the CIGS deposition process was further adapted to the mild steel substrate with electrodeposited Ni/Cr bi-layer barrier coating by engineering the evaporation profiles of In and Ga in the different stages at maximum nominal

substrate temperatures of 450 °C. An additional RbF post deposition treatment was used to further improve the cell performance resulting in certified efficiency of 18.0 % (with MgF_2 anti reflective coating) (see Fig. 5).

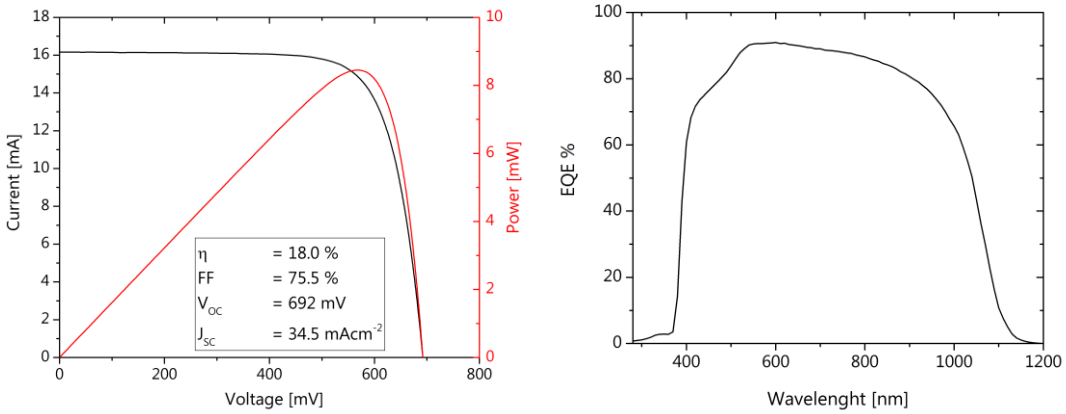

Fig. 5 Left) Certified I-V and power output curves of a solar cell on Ni/Cr coated mild steel foil with V_{OC} 692 mV, J_{SC} 34.5 mA/cm^2, FF 75.5 and efficiency of 18.0 % on a 0.469 cm^2 area cell measured at the Fraunhofer ISE institute. Right) External quantum efficiency of the cell measured at Fraunhofer ISE.

5. Conclusion

CIGS solar cells were grown on mild steel substrates with an electrochemically plated Ni/Cr bi-layer using a low temperature multistage co-evaporation process for CIGS. A certified efficiency of 18.0 % was achieved by applying a NaF and RbF post deposition treatment proving that high efficiency CIGS solar cells can be grown on mild steel foils. In this study we show that a roll to roll compatible and industrially scalable Ni/Cr protection bi-layer on mild steel substrate can sufficiently suppress the diffusion of detrimental elements from the substrate into the CIGS if the nominal substrate temperature does not exceed 500 °C. For higher substrate temperatures an impurity induced deep defect around 0.33 eV was found to cause non-radiative recombination losses. A more precise control of the processing temperature would allow designing a

distinct substrate temperature profile for growing CIGS on mild steel substrates. However, the In and Ga evaporation profiles must also be engineered accordingly. This approach is considered to be most promising for enhancing the absorber growth on mild steel substrates.

Acknowledgement

Financial funding from the Swiss Federal Commission for Technology and Innovation CTI, Project Nr. *17747.2 PFIW-IW* is gratefully acknowledged. We are also grateful to the Laboratory for Nancoscale Material Science at Empa Duebendorf for providing access to their ToF-SIMS system for our studies.

References

A. Chirila, P.B., F. Pianezzi, S.Seyerling, A.R. Uhl, S. Buecheler, S. Nishiwaki, A.N. Tiwari, 2011. Development of high efficiency flexible CIGS solar cells on different substrates, 21st International Photovoltaic Science and Engineering Conference. Fukukoka, Japan.

Bae, D., Kwon, S., Oh, J., Kim, W.K., Park, H., 2013. Investigation of Al2O3 diffusion barrier layer fabricated by atomic layer deposition for flexible Cu(In,Ga)Se2 solar cells. Renewable Energy 55, 62-68.

Blosch, P., Chirila, A., Pianezzi, F., Seyrling, S., Rossbach, P., Buecheler, S., Nishiwaki, S., Tiwari, A.N., 2011. Comparative Study of Different Back-Contact Designs for High-Efficiency CIGS Solar Cells on Stainless Steel Foils. Ieee Journal of Photovoltaics 1(2), 194-199.

Chirila, A., Reinhard, P., Pianezzi, F., Bloesch, P., Uhl, A.R., Fella, C., Kranz, L., Keller, D., Gretener, C., Hagendorfer, H., Jaeger, D., Erni, R., Nishiwaki, S., Buecheler, S., Tiwari, A.N., 2013. Potassium-induced surface modification of Cu(In,Ga)Se-2 thin films for high-efficiency solar cells. Nat. Mater. 12(12), 1107-1111.

Cho, D.-H., Chung, Y.-D., Lee, K.-S., Kim, K.-H., Kim, J.-H., Park, S.-J., Kim, J., 2013. Photovoltaic performance of flexible Cu(In,Ga)Se2 thin-film solar cells with varying Cr impurity barrier thickness. Current Applied Physics 13(9), 2033-2037.

Eisenbarth, T., Caballero, R., Kaufmann, C.A., Eicke, A., Unold, T., 2012. Influence of iron on defect concentrations and device performance for Cu(In,Ga)Se2 solar cells on stainless steel substrates. Prog. Photovoltaics 20(5), 568-574.

Eisenbarth, T., Unold, T., Caballero, R., Kaufmann, C.A., Schock, H.-W., 2010. Interpretation of admittance, capacitance-voltage, and current-voltage signatures in Cu(In,Ga)Se2 thin film solar cells, J. Appl. Phys. p. 034509.

Herz, K., Eicke, A., Kessler, F., Wächter, R., Powalla, M., 2003. Diffusion barriers for CIGS solar cells on metallic substrates. Thin Solid Films 431, 392-397.

Jackson, P., Wuerz, R., Hariskos, D., Lotter, E., Witte, W., Powalla, M., 2016. Effects of heavy alkali elementsin Cu(In,Ga)Se-2 solar cells with efficiencies up to 22.6%. Phys. Status Solidi-Rapid Res. Lett. 10(8), 583-586.

Liu, W.-S., Hu, H.-C., Pu, N.-W., Liang, S.-C., 2015. Developing flexible CIGS solar cells on stainless steel substrates by using Ti/TiN composite structures as the diffusion barrier layer. Journal of Alloys and Compounds 631, 146-152.

Losee, D.L., 1975. Admittance spectroscopy of impurity levels in Schottky barriers. Journal of Applied Physics 46(5), 2204-2214.

Nishiwaki, S., Feurer, T., Bissig, B., Avancini, E., Carron, R., Buecheler, S., Tiwari, A., 2017. Precise Se-flux control and its effect on Cu(In,Ga)Se 2 absorber layer deposited at low substrate temperature by multi stage co-evaporation. Thin Solid Films 633(supplement), 18-22.

Pianezzi, F., Chirila, A., Blosch, P., Seyrling, S., Buecheler, S., Kranz, L., Fella, C., Tiwari, A.N., 2012. Electronic properties of Cu(In,Ga)Se2 solar cells on stainless steel foils without diffusion barrier. Prog. Photovoltaics 20(3), 253-259.

Pianezzi, F., Nishiwaki, S., Kranz, L., Sutter-Fella, C.M., Reinhard, P., Bissig, B., Hagendorfer, H., Buecheler, S., Tiwari, A.N., 2015. Influence of Ni and Cr impurities on the electronic properties of Cu(In,Ga)Se-2 thin film solar cells. Prog. Photovoltaics 23(7), 892-900.

Walter, T., Herberholz, R., Müller, C., Schock, H.W., 1996. Determination of defect distributions from admittance measurements and application to Cu(In,Ga)Se2 based heterojunctions. Journal of Applied Physics 80(8), 4411-4420.

Weiss, T.P., Nishiwaki, S., Bissig, B., Carron, R., Avancini, E., Johannes, L., Buecheler, S., Tiwari, A.N., 2017. Injection current barrier formation for RbF post deposition treated Cu(In,Ga)Se2 based solar cells. (accepted).

Werner, F., Wolter, M.H., Siebentritt, S., Sozzi, G., Di Napoli, S., Menozzi, R., Jackson, P., Witte, W., 2017. Alkalie treatment of Cu(In,Ga)Se_2 thin film absorbers: transport barriers and their influence on the admittance spectrum. (unpublished).

Wuerz, R., Eicke, A., Frankenfeld, M., Kessler, F., Powalla, M., Rogin, P., Yazdani-Assl, O., 2009. CIGS thin-film solar cells on steel substrates. Thin Solid Films 517(7), 2415-2418.

Wuerz, R., Eicke, A., Kessler, F., Pianezzi, F., 2014. Influence of iron on the performance of CIGS thin-film solar cells. Sol. Energy Mater. Sol. Cells 130, 107-117.